Hydrogen-Bonded Water-Aminium Assemblies for Synthesis of Zeotypes with Ordered Heteroatoms.

Sung Hwan Park[†], Sambhu Radhakrishnan[‡,§], Wanuk Choi[†], C. Vinod Chandran[‡,§], Kingsley Christian Kemp[†], Eric Breynaert[‡,§], Robert G. Bell[^], Christine E. A. Kirschhock[‡], and Suk Bong Hong[†,*]

[†] Center for Ordered Nanoporous Materials Synthesis, Division of Environmental Science and Engineering, POSTECH, Pohang 37673, Korea.

[‡] Center for Surface Chemistry and Catalysis, Characterization and Application Team (COK-kat), Celestijnenlaan 200 F – box 2461, KU Leuven, 3001 Heverlee, Belgium.

[§] NMRCoRe, Celestijnenlaan 200 F – box 2461, KU Leuven, 3001 Heverlee, Belgium.

[^] Department of Chemistry, University College London, 20 Gordon Street, London WC1H 0AJ, UK.

ABSTRACT: Water plays a central role in the crystallization of a variety of organic, inorganic, biological, and hybrid materials. This is also true for zeolites and zeolite-like materials, an important class of industrial catalysts and adsorbents. Water is always present during their hydrothermal synthesis, either with or without organic species as structure-directing agents. Apart from its role as solvent or catalyst, structure direction by water in zeolite synthesis has never been clearly elucidated. Here we report the crystallization of phosphate-based molecular sieves using rationally designed, hydrogen-bonded water-aminium assemblies, resulting in molecular sieves exhibiting the crystallographic ordering of heteroatoms. We demonstrate that a 1:1 assembly of water and diprotonated *N*,*N*-dimethyl-1,2-ethanediamine acts as a structure-directing agent in the synthesis of a silicoaluminophosphate material with phillipsite (PHI) topology using SMARTER crystallography combining single-crystal X-ray diffraction and nuclear magnetic resonance spectroscopy as well as *ab initio* molecular dynamics, Raman and Infrared spectroscopies. The molecular arrangement of the hydrogen-bonded assembly matches well with the shape and size of subunits in the PHI structure, and their charge distributions result in the strict ordering of framework tetrahedral atoms. This concept of structure direction by water-containing supramolecular assemblies should be applicable to the synthesis of many classes of porous materials.

■ INTRODUCTION

A wide variety of organic amines and quaternary ammonium ions are used as structure-directing agents (SDAs) in the synthesis of zeolites and molecular sieves[1,2]. Their structure-directing effect is mainly ascribed to weak, non-covalent interactions with the inorganic polymeric species in the synthesis mixture[3]. Presumably, these interactions arise from successive replacement of water molecules in the solvation shell of the SDAs by oxygen atoms from the evolving inorganic network[4,5]. Over time, sufficiently ordered domains, related to the final periodic structure, form and ripen[4,6]. Water readily forms hydrogen bonds with proton acceptors or donors, and the structure of liquid water itself is determined by this phenomenon. Locally and transiently, this leads to dynamic water clusters with a wide range of order[7,8], which are even more difficult to characterise when they are confined in nanopores[9,10]. Hence, while water is integral to every hydrothermal zeolite crystallization, it is daunting to discern a local, structure-directing effect from its global role as solvent or catalyst. One option to examine this previously unexplored role of water is to identify persisting assemblies of water with organic molecules as supramolecular SDAs in as-synthesized zeolites and zeotypes.

The synthesis of phosphate-based molecular sieves, such as aluminophosphates ($AlPO_4$'s), silicoaluminophosphates (SAPOs), and metalloaluminophosphates (MeAPOs), involves an appropriate P source, commonly in the form of *o*-phosphoric acid leading to lower pH synthesis gels compared to (alumino)silicates[11-13]. In this study, a synthesis pH was selected that was high enough to exploit mineralization by hydroxyl ions, while still ensuring nominal double protonation of diamines, known for their strong hydrogen bonds[14-17]. These hydrogen-bonded water-aminium assemblies should be stable enough to persist during zeolite synthesis conditions and can be expected to act as real SDAs[1,18,19], with the protonated diamines compensating the negative framework charges arising from the presence of heteroatoms such as Si or Mg in the zeotypes.

Hydrophilic, short-chain (C2-C3) diamines with varying *N*-methylation were selected to probe both steric and thermodynamic effects, owing to variations in pK_a value, as well as the presence of different numbers of hydrogen atoms available for hydrogen bonding[15,20]. These diamines are also well-known for their proficiency to form co-crystals[21,22], indicating a high affinity to form stable associations through hydrogen bonding. Our selections of the diamines for SAPO syntheses were made with respect to the combinations of tertiary and primary amine groups attached to the carbon chains, thus giving either symmetric or asymmetric configurations. Here we show that water can strongly hydrogen bond with protonated aliphatic diamines to form supramolecular assemblies that direct the synthesis of

SAPO molecular sieves with ordered framework tetrahedral atoms (T-atoms). We have also demonstrated a strict correlation between the molecular arrangements of the intrazeolitic water-aminium assemblies and framework Si distributions.

■ EXPERIMENTAL SECTION

SAPO molecular sieve syntheses. In a typical synthesis of SAPO-PHI and SAPO-CHA, 0.58 g of pseudoboehmite (PB) (Catapal B, Vista) was added to the solution of 0.93 g of *N*,*N*-dimethyl-1,2-ethanediamine (DMEDA) (95%, Aldrich) and 6.42 g of deionized water under continuous stirring. After dropwise addition of 0.86 g of *o*-phosphoric acid (85%, Aldrich) and 0.56 g of colloidal silica (Ludox AS-40, DuPont), the mixture was stirred for 1 h to prepare a homogenous gel. The resulting mixture was charged into rotating Teflon-lined autoclaves (60 rpm) and heated at 150 °C for 12 days and at 180 ºC for 2 days to obtain SAPO-PHI and SAPO-CHA, respectively. SAPO-GIS was synthesized by replacing DMEDA with an equimolar amount (1.03 g) of *N*,*N*-dimethyl-1,3-propanediamine (DMPDA) (98%, Aldrich) in the above gel followed by heating at 150 °C for 12 days. After crystallization, the solid product was collected by filtration, repeatedly washed with deionized water and then dried overnight at room temperature.

General characterization. Powder X-ray diffraction (XRD) patterns were collected in flat plate mode using a PANalytical X'Pert diffractometer (Cu Kα radiation) with an X'Celerator detector. Elemental analysis was obtained by the Pohang Institute of Metal Industry Advancement. Thermogravimetric and differential thermal analyses were performed in air on a SII EXSTAR 6000 thermal analyser. Crystal morphology and average size were determined using a JEOL JSM-6510 scanning electron microscope. Infrared (IR) spectra were recorded on a Thermo-Nicolet 6700 Fourier-transform (FT)-IR spectrometer equipped with an MCT detector and a home-built IR cell with CaF_2 windows. Raman spectra were measured on a Bruker FRA106/S FT-Raman spectrometer equipped with a Nd:YAG laser operating at 1064 nm.

Single-crystal XRD analysis. Synchrotron single-crystal XRD data were measured at -173 °C on the 2D beamline of the PAL, using an ADSC Q210 CCD area detector and monochromated X-ray source. The raw data was processed and scaled using the HKL3000 and DENZO programs[23], and the space group was determined utilizing the XPREP program[24]. The structure was solved by direct methods[25], and the structure refinement was carried out with full-matrix least-squares refinements on F^2 using the SHELXL2018 program[26]. All framework atoms and extra-framework species were located from the difference Fourier map (F_o-F_c), and all non-hydrogen atoms were refined anisotropically. Crystal data and details of structure determination are given in Supplementary Information.

Solid-state nuclear magnetic resonance (NMR) spectroscopy. Solid-state NMR experiments were carried out on Bruker Neo 800 and Bruker Avance 500 NMR spectrometers, operating at magnetic field strengths of 18.8 (801.25 MHz ^{1}H Larmor frequency) and 11.7 (500.87 MHz ^{1}H Larmor frequency) T, respectively. Magic angle spinning (MAS) NMR experiments were performed using a Bruker 4 mm or a 1.9 mm triple resonance MAS probe. The samples were D_2O-exchanged, dried in a dessicator over P_2O_5 and then packed in zirconia rotors. More detailed 1D (^{31}P, ^{1}H, ^{29}Si, and ^{27}Al) and 2D (^{31}P double quantum–single quantum (DQ-SQ) and ^{1}H-^{31}P heteronuclear correlation (HETCOR), ^{31}P-^{27}Al HETCOR, and ^{1}H-^{27}Al HETCOR) MAS NMR measurement conditions can be found in Supporting Information.

***ab initio* molecular dynamics (AIMD) simulations.** The simulations were carried out using the program CP2K[27,28], which utilizes a combined Gaussian-Plane Wave (GPW) approach. The PBE functional was used together with the DZVP-MOLOPT-SR-GTH basis set for all atoms. Core electrons were represented by the GTH pseudopotentials. All AIMD runs were performed at 27 °C in the NVT ensemble, assuming no internal symmetry. Each simulation had a duration of at least 20 ps using a 0.5 fs time step. Two framework models were used based on i) the T-atoms distribution of the $P2_1/c$ structure, which consists of strictly alternating Si- and P-*dcc* units and ii) a less ordered structure where two Al-P pairs, bridging the alternate *dcc*s, are each replaced by two Si atoms, consistent with the MAS NMR data. In the latter case, the framework composition was thus $Al_{14}P_6Si_{12}O_{64}$. In the simulations reported here, each simulation cell contained four SDA species, one per *t-phi* cage. The SDA moieties were represented as $[H_2O\text{-}(DMEDA{\cdot}H_2)]^{2+}$, i.e., one water molecule per diaminium ion, associated with the tertiary aminium as characterized by single-crystal X-Ray crystallography. Separate simulations were carried out for each framework configuration, in which the $(DMEDA{\cdot}H_2)^{2+}$ ions were either all in the major orientation, or all in the minor one. Atomic positions and ensemble energies were sampled at intervals of 100 fs throughout the simulations. The orientations of the primary aminium with respect to the methylene C-C bond were monitored and defined as being in the staggered or eclipsed conformation with respect to the neighboring methylene C-C bond, depending on the H-C-N-H torsional angles.

■ RESULTS AND DISCUSSION

Table 1 lists the representative SAPO molecular sieves obtained using synthesis mixtures with compositions $(1.0\text{-}4.0)R{\cdot}1.00Al_2O_3{\cdot}0.75P_2O_5{\cdot}0.75SiO_2{\cdot}80H_2O$, where R is a short-chain diamine and the low water concentration assured its intimate interaction with the organic component (Experimental Section). Hereafter, the products are named as SAPO-FTC, where FTC specifies the framework type code[2]. With a $DMEDA/Al_2O_3$ ratio fixed to 2.0, highly crystalline SAPO-PHI was obtained after heating under rotation (60 rpm) at 150 °C for 12 days (Figure S1). Altering the $DMEDA/Al_2O_3$ ratio away from 2.0 resulted in a product that was not phase pure. Also, the addition of a small amount of HNO_3 or NH_4OH led to notable product changes, even with adjusted pH. In particular, while the formation of SAPO-PHI or SAPO-CHA from the gel (no. 3 in Table 1) was still observed despite the significant change in the initial pH (10.0) of synthesis mixtures, the addition of HNO_3 into the same gels (no. 7) to adjust the gel pH to be equal to that (8.0) of the gel (no. 2) apparently inhibited the crystallization of those SAPO materials. On the other hand, the presence of NH_4^+ ions in the SAPO gel (no. 6) where the gel pH was kept to 8.0, like the case of the gel (no. 2), also disturbed the formation of any SAPO materials. This inhibition of SAPO-PHI crystallization by proton-donor or -acceptor, i.e., NH_4^+ or NO_3^- ion which cannot be considered as a SDA, suggests that the structure direction depends on the intimate hydrogen bonding between water and diamine molecules.

Table 1. Representative synthesis results[a]

		Gel composition		Product[c]	
Gel no.	pH_{gel}[b]	R	*x*	Temperature/time = 150 °C/12 days	Temperature/time = 180 °C/2 days
1	5.5	DMEDA	1.0	L	SAPO-GIS + SAPO-SOD
2	8.0	DMEDA	2.0	SAPO-PHI	SAPO-CHA
3	10.1	DMEDA	4.0	SAPO-PHI + A	SAPO-CHA + (L)
4	5.4[d]	DMEDA	2.0	A	D + L
5	10.0[d]	DMEDA	2.0	L + (SAPO-PHI)	A + L
6	8.0[e]	DMEDA	1.0	L	L
7	8.0[e]	DMEDA	4.0	A + SAPO-PHI	L + SAPO-CHA
8	8.5	TMEDA	2.0	SAPO-GIS + SAPO-CHA	SAPO-CHA + (SAPO-GIS)
9	8.8	$ATMEA^+$	2.0	D + (SAPO-PHI)	SAPO-SOD + (SAPO-PHI)
10	8.1	DMPDA	2.0	SAPO-GIS + (L)	SAPO-GIS
11	8.3	TMPDA	2.0	SAPO-GIS + (SAPO-CHA)	SAPO-GIS

[a]The chemical composition of the SAPO gels used is xR•1.00Al_2O_3•0.75P_2O_5•0.75SiO_2•80H_2O, where x is varied between $1.0 \leq x \leq 4.0$, and R is *N*,*N*-dimethyl-1,2-ethanediamine (DMEDA), *N*,*N*,*N*´,*N*´-tetramethyl-1,2-ethanediamine (TMEDA), 2-amino-*N*,*N*,*N*-trimethylethanaminium ($ATMEA^+$), *N*,*N*-dimethyl-1,3-propanediamine (DMPDA), or *N*,*N*,*N*´,*N*´-tetramethyl-1,3-propanediamine (TMPDA). [b]The initial pH of each gel. [c]The phase appearing first is the major phase, and the product obtained in a trace amount is given in parentheses. A, D, and L are amorphous, dense, and layered phases, respectively. [d]While the gel composition is the same as that of gel no. 2, the pH_{gel} of gel nos. 4 and 5 was adjusted by adding a small amount of HNO_3 and NH_4OH, respectively. [e]While the gel composition is the same as that of gel nos. 1 and 3, the pH_{gel} of gel nos. 6 and 7 was adjusted by adding a small amount of NH_4OH and HNO_3, respectively.

IR and Raman spectroscopy confirmed strong hydrogen bonding between water and fully protonated DMEDA [$(DMEDA{\cdot}H_2)^{2+}$] in as-synthesized SAPO-PHI (Figure S2). Also, ^{1}H-^{1}H radio frequency-driven recoupling (RFDR) and ^{1}H-^{1}H exchange spectroscopy (EXSY) MAS NMR showed the existence of dipolar coupling and chemical exchange between the aminium and water protons (Figures S3 and S4), further confirming the hydrogen-bonding network. This and its unusual framework composition (Si/(Si+Al+P) = 0.24 and P/Si = 1.13 indicating the presence of a highly ordered SAPO domain; Table S1) prompted an NMR-crystallography approach, combining XRD, 1D and 2D MAS NMR and molecular modelling (Figures 1a-1c). A highly ordered T-atom distribution (Figure 1d), including an isomorphous substitution scheme (Figure 1e), was uncovered. 1D ^{29}Si MAS NMR of as-synthesized SAPO-PHI revealed the majority of Si (80%) to be linked to four AlO_4^- tetrahedra (Q^{44}; Q^{4n} stands for the tetrahedrally coordinated Si atoms with *n*Al and (4-*n*)Si neighbor atoms, where n = 0, 1, 2, 3, or 4), with only an insignificant fraction of Al (^{27}Al MAS NMR) being connected to four SiO_4 tetrahedra (Figures S5 and S6). Therefore, the occurrence of large aluminosilicate domains next to $AlPO_4$ zones could be excluded. The ^{31}P direct excitation (DE) and ^{31}P-^{27}Al CP-HETCOR MAS NMR data indicated the presence of at least five distinct P sites (I-V). According to ^{31}P DQ-SQ MAS NMR spectroscopy (Figure 1b), these resonances self- and cross-correlate, implying their mutual proximity. All these observations hinted at P-rich structural units next to Si-rich ones. The simplest motif consistent with these results and framework topology are single 4-rings (S4Rs) with two Al atoms and either two P or two Si atoms, each. The combination of self-and cross-correlations of the P sites further implied that P-containing S4Rs occur edge-connected, resulting in the double crankshaft chain (*dcc*) encountered in the PHI topology (Figure S7).

A plausible model, in agreement with all experimental data, for the SAPO-PHI framework contains strictly alternating aluminosilicate-like *dcc*s (Si-*dcc*s) with an Si/Al ratio of unity, next to $AlPO_4$-like *dcc*s (P-*dcc*s) (Figures 1d and 1e). The resulting space group $P2_1/c$ is a subgroup of the *Cc* setting, obtained from fast indexing of its powder XRD pattern (Figure S1). In this structure, two crystallographically distinct Si sites connect to two distinct Al sites (Al^a and Al^b) having three Si and one P neighbors (Si-*dcc*), while two distinct P sites (P^I and P^{IV}) link to two additional Al atoms (Al^c and Al^d), each having one Si and three P neighbors. Single-crystal structure refinement confirmed this model and also revealed that each *t-phi* cage contains one hydrogen-bonded water-aminium assembly ($[H_2O$-$(DMEDA{\cdot}H_2)]^{2+}$) (Experimental Section, Figure 2, and Tables S2-S6), implying its role as an SDA in SAPO-PHI synthesis. Interestingly, two different assembly orientations were found in a major/minor ratio of 80:20, also in accordance with ^{1}H-^{13}C CP MAS NMR (Figure S8). Both showed direct interaction of the primary aminium of $[H_2O$-$(DMEDA{\cdot}H_2)]^{2+}$ with the single 8-ring (S8R) connecting 8-hedral ($[4^58^3]$) *t-oto* and 12-hedral ($[4^78^5]$) *t-phi* cages in the *b*-axis. The tertiary aminium is located roughly centered in *t-phi*, with the methyl

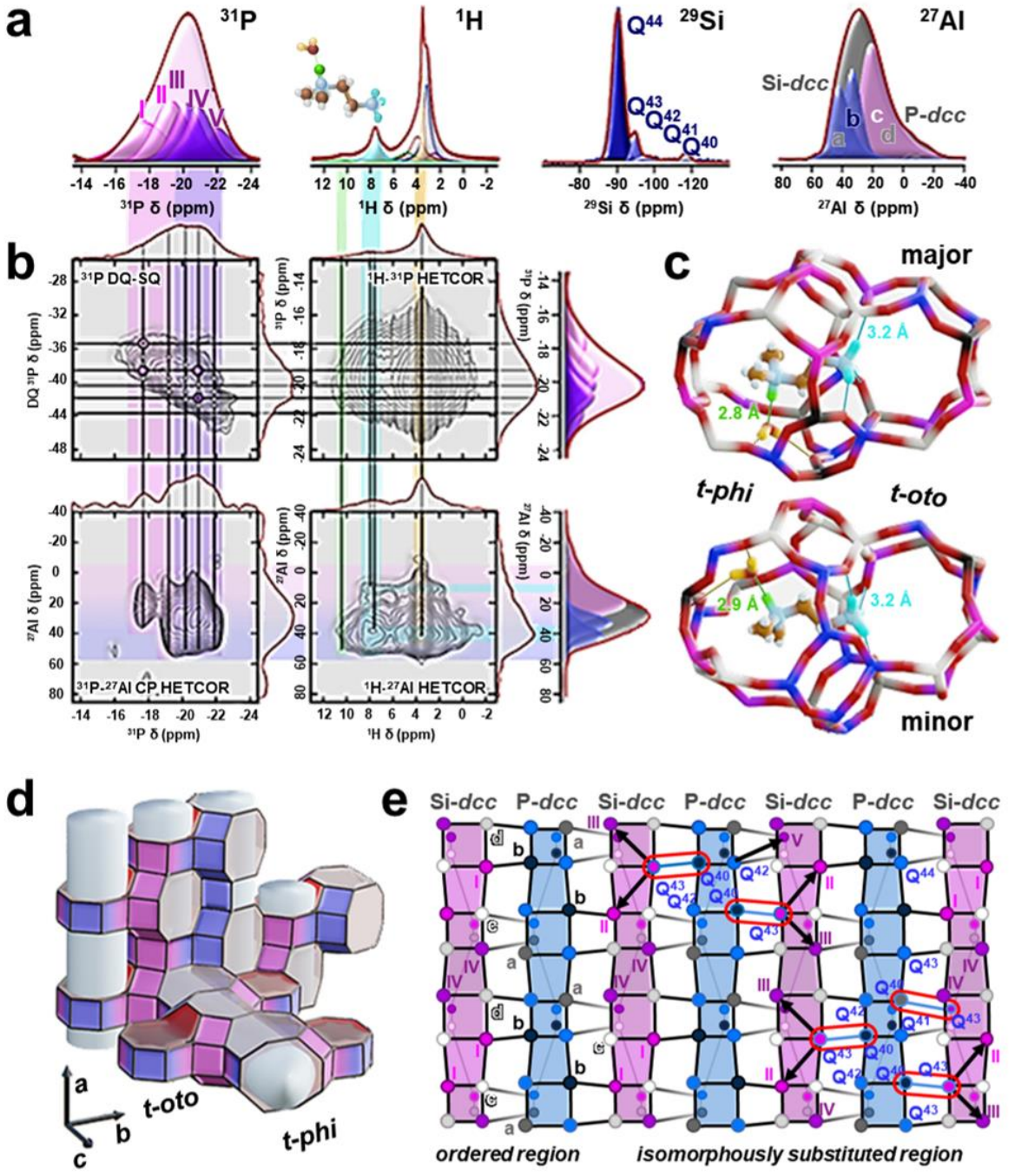

Figure 1. Structural characterization of SAPO-PHI. (a) 1D ^{31}P, ^{1}H, ^{29}Si, and ^{27}Al and (b) 2D ^{31}P DQ-SQ and ^{1}H-^{31}P HETCOR, ^{31}P-^{27}Al HETCOR, and ^{1}H-^{27}Al HETCOR MAS NMR spectra of as-synthesized SAPO-PHI. Projections are shown on the top and right of every panel. MAS NMR spectra are duplicated for convenient comparison. (c) Molecular modelling of site and orientation of $[H_2O\text{-}(DMEDA{\cdot}H_2)]^{2+}$ in ordered (top) and isomorphously substituted (bottom) frameworks. (d) PHI topology and ordering of its dcc units. (e) Projection of PHI framework illustrating the connectivity in ordered and isomorphous substitution scheme. Color codes for (c): protons, given in (a); framework, given in (e).

groups pointing towards the two neighboring *t-oto* cages along the *a*-axis (Figures 1c and 1d). These two orientations of $[H_2O\text{-}(DMEDA{\cdot}H_2)]^{2+}$ differ in the direction of their tertiary aminium protons, pointing towards the associated water molecule located in one of the two S8Rs of neighboring *t-phi* cages, in either positive or negative *c*-direction. The occupation numbers for the two orientations closely mirror the overall framework Si distribution derived by MAS NMR (Figures 1a and S9), with 80% Q^{44} and 20% of Si connected with at least one Si.

Although a strict ordering scheme of undisturbed Si- and P-*dcc* units cannot account for the four ^{29}Si resonances (i.e., Q^{43},

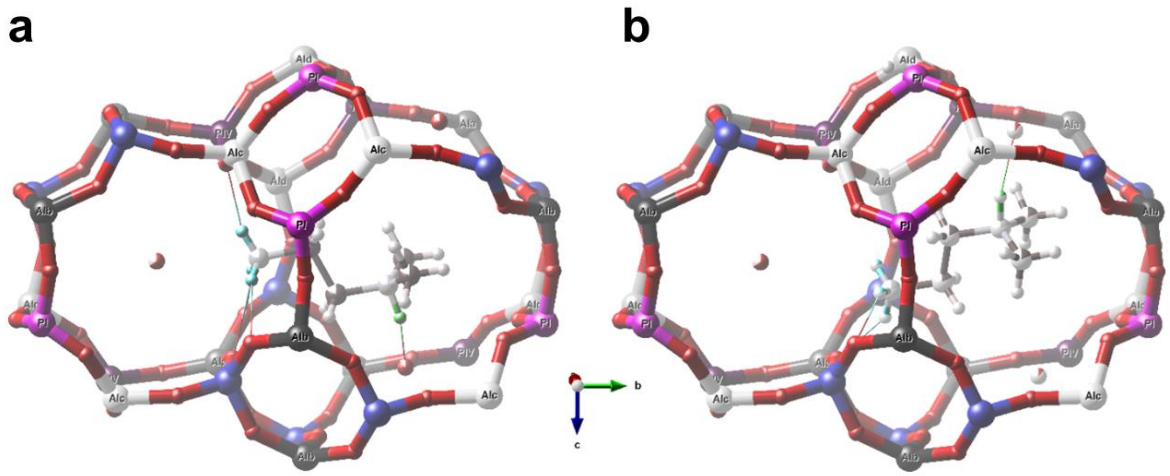

Figure 2. Structures of $[H_2O\text{-}(DMEDA{\cdot}H_2)]^{2+}$ in as-synthesized, hydrated SAPO-PHI. A combination of single-crystal X-ray crystallography, MAS NMR spectroscopy, and AIMD simulations was employed to determine these structures with (a) major and (b) minor orientations with a relative ratio of 80:20. Color codes: C, brown; N, light grey; O, red; hydrogen-bonded H, cyan or green. In the major and minor orientations of the hydrogen-bonded water-aminum assembly, protonated DMEDA is pointing with the tertiary aminium group in opposite directions along the *c*-axis. Each tertiary aminium proton is found within hydrogen-bonding distance to the water molecule located in the S8R connecting two adjacent *t-phi* cages. The primary aminium group of $[H_2O\text{-}(DMEDA{\cdot}H_2)]^{2+}$ is located within hydrogen-bonding distance to the framework, specifically to the S8R connecting the *t-phi* to the *t-oto* cage in the *b*-axis. The oxygen atoms, viz. water molecules, residing at the center of *t-oto* cages disappear after dehydration under a vacuum (10^{-4} kPa at 200 °C for 6 h).

Q^{42}, Q^{41}, and Q^{40}), nor for the five ^{31}P resonances (Figures S9 and S10), isomorphous substitution of P and/or Al by Si readily explains the occurrence of these sites. The simplest isomorphous substitution scheme, preserving net framework charge, replaces Al-P pairs connecting Si- and P-*dcc*s by Si-Si pairs (Figure 1e). Here, the framework charge distribution is rearranged, while keeping the number of $[H_2O\text{-}(DMEDA{\cdot}H_2)]^{2+}$ largely unaffected. To verify this and fully assign the MAS NMR spectra (Figures 1a and 1b), periodic AIMD simulations were performed. Within 32 T-atom simulation cells of a SAPO-PHI framework with strictly alternating Si- and P-*dcc*s, the two different $[H_2O\text{-}(DMEDA{\cdot}H_2)]^{2+}$ orientations suggested by single-crystal X-ray crystallography were found to interact differently with local framework environments (Figure 1c and Experimental Section).

Throughout all simulations, strong hydrogen bonding between the tertiary aminium proton and the water oxygen occurred for both orientations, and the water molecule always oriented its hydrogen atoms towards framework oxygen atoms of charged aluminosilicate regions. The primary aminium of $[H_2O\text{-}(DMEDA{\cdot}H_2)]^{2+}$ directly interacted with framework oxygen atoms via hydrogen bonds. In ordered regions of the structure (Figure 1e), the major orientation (Figure 1c, top) allows the primary aminium protons to adopt the preferred staggered conformation with respect to the methylene C-C bond. This enables the two hydrogens of the primary aminium to interact with the framework oxygen atoms of Si-*dcc* (Movie S1), which is not possible for the minor orientation and could only be achieved in an unfavourable eclipsed state. The significant energy difference of +40.6 kJ (mol unit cell)$^{-1}$ observed for the minor orientation, compared to the major one, in the fully ordered structure clearly shows that within the ordered region of SAPO-PHI, the major arrangement occurs exclusively (Figures S11 and S12, and Table S7).

The isomorphous substitution scheme, suggested by NMR-crystallography, was investigated for its impact on the orientation of $[H_2O\text{-}(DMEDA{\cdot}H_2)]^{2+}$. The Si-Si replacement of Al-P pairs, connecting *dcc*s in the *c*-axis, can create all-Si S4Rs and aluminosilicate (Si/Al = 1.0) ones in Si- and P-*dcc* units, respectively, locally reversing the charge distribution. In cages with the inverted charge distribution, the minor orientation assumes a staggered conformation, allowing two of the three primary aminium protons to interact with oxygen atoms in aluminosilicate domains. Therefore, it is clear that hydrogen bonding of the primary aminium with framework oxygen atoms determines the orientation of $[H_2O\text{-}(DMEDA{\cdot}H_2)]^{2+}$: the major orientation is predominant in ordered regions and the minor orientation in isomorphously substituted regions with the inverted charge distribution. These results are in excellent agreement with the structure of $[H_2O\text{-}(DMEDA{\cdot}H_2)]^{2+}$ derived by NMR-crystallography (Figure 2). Substituting 5.5% of Al-P pairs in the P-dcc provides an almost perfect agreement between the measured and modelled ^{29}Si intensities (Figure S9), and a consistent, quantitative assignment of the ^{31}P signals based on the bonding angles of P-linked oxygen atoms (Figure S10). The corroboration between MAS NMR and AIMD results was further confirmed by ^{1}H-^{27}Al HETCOR MAS NMR spectroscopy. The proton associated with the tertiary aminium group exclusively interacts with the Al atoms belonging to Si-*dcc*, through its hydrogen-bonded water. This results in a through-space correlation between this proton and Al in Si-*dcc*. The protons associated with the primary aminium directly interact with Al atoms belonging to the Si- and P-*dcc*s, causing a significantly stronger correlation with both sites in the ^{1}H-^{27}Al HETCOR MAS NMR spectrum (Figure 1b; cyan and green traces).

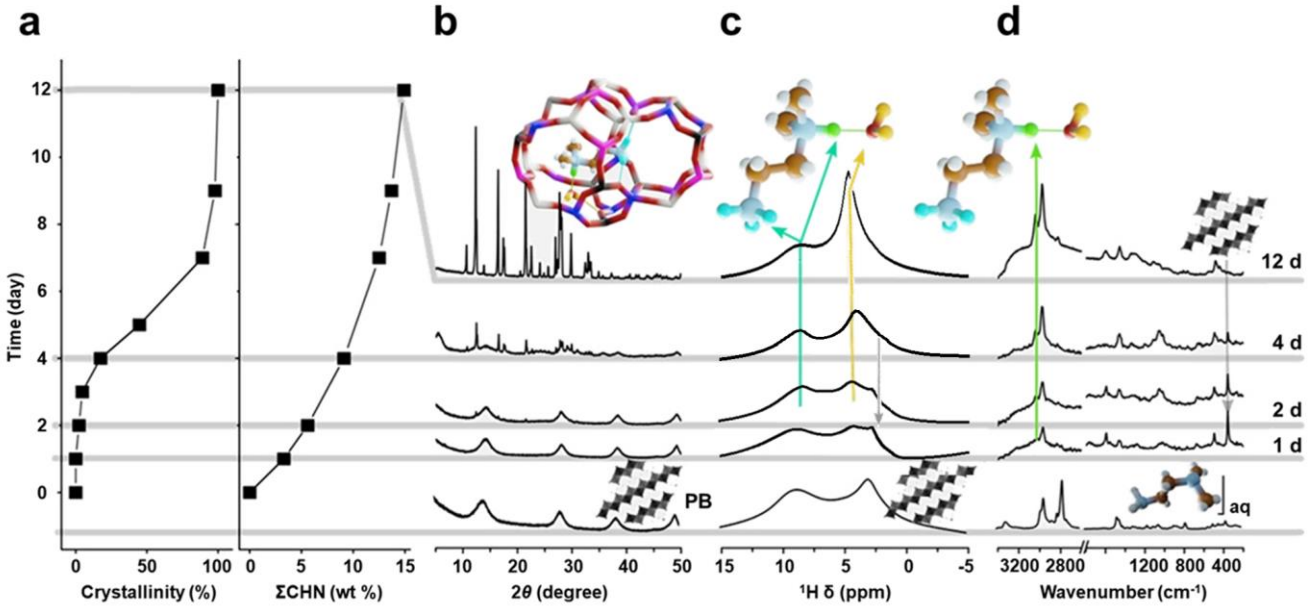

Figure 3. Crystallization kinetics of SAPO-PHI. (a) Relative crystallinities and organic contents at different crystallization times determined by powder XRD and elemental analyses, respectively, (b) powder XRD patterns, and (c) ^{1}H MAS NMR and (d) Raman spectra of a series of solid products isolated after heating at 150 °C for 1 – 12 days. The crystallinities at different crystallization times were assessed by referencing the relative intensities to the height of an X-ray peak at 2θ = 12.4°. Powder XRD and Raman data were obtained from hydrated solids, ^{1}H MAS NMR data were collected from D_2O exchanged samples, dehydrated under a vacuum (10^{-4} kPa at 200 °C for 2 h). The bottom traces show powder XRD pattern and ^{1}H MAS NMR spectrum of PB, and the Raman spectrum of DMEDA in aqueous solution.

To check whether the $[H_2O\text{-}(DMEDA{\cdot}H_2)]^{2+}$ in SAPO-PHI persists even at higher temperatures, we carried out periodic AIMD simulations at 150 °C, the SAPO-PHI crystallization temperature. At all time steps of simulations, the hydrogen bond (O···H) distances of the oxygen and proton of water and the tertiary aminium group in DMEDA, respectively, were calculated to lie within the range of 1.30 – 2.69 Å, showing the persistence of 1:1 hydrogen-bonded water-aminium assemblies (Figure S13 and Table S8). While these distances increase at 200 °C, in addition, neither exchange nor migration of the water molecule in $[H_2O\text{-}(DMEDA{\cdot}H_2)]^{2+}$ was observed. Therefore, it can be concluded that the hydrogen-bonded water molecule is an irreplaceable part of the supramolecular assemblies which direct the synthesis of SAPO-PHI.

The detailed and quantitative structure solution of $[H_2O\text{-}(DMEDA{\cdot}H_2)]^{2+}$ (Figure 2) also shows that the primary aminium interacts with the PHI framework in a direct and element-specific manner, whereas the tertiary aminium proton does so only by mediation of strongly hydrogen-bonded water molecules. The observation of the highly ordered SAPO-PHI is of particular interest, because the asymmetric preference of tertiary and primary aminium in $[H_2O\text{-}(DMEDA{\cdot}H_2)]^{2+}$ for water or charged framework atoms conforms to an asymmetric *t-oto* ($[4^5 8^3]$) and *t-phi* ($[4^7 8^5]$) arrangement in the framework. In contrast, CHA and GIS structures can both be assembled with only one symmetric cage type (*t-cha* ($[4^{12}6^2 8^6]$) and *t-gis* ($[4^6 8^4]$) cages, respectively). While both SAPO materials also show the presence of strongly hydrogen-bonded water molecules even after dehydration under a vacuum (10^{-4} kPa at 200 °C for 6 h, Figure S14), indeed, no such strict preference of either tertiary or primary aminium groups to hydrogen bond with a water molecule was observed, requiring both aminium groups to show similar interactions with water and/or the SAPO framework (Figures S14-S18 and Tables S9-S19).

Interestingly, the formation of SAPO-CHA and SAPO-GIS was achieved using not only the asymmetric diamines but also symmetric ones, whereas SAPO-PHI was obtained by the exclusive use of asymmetric DMEDA. For example, the use of symmetric *N*,*N*,*N´*,*N´*-tetramethyl-1,2-ethanediamine (TMEDA) or *N*,*N*,*N´*,*N´*-tetramethyl-1,3-propanediamine (TMPDA) always led to the formation of zeotype structures with CHA and/or GIS topologies (Table 1). However, we found some exceptions where the phase selectivity of crystallization cannot be rationalized in terms of symmetry of the organic compound itself only. Unlike the case of asymmetric DMEDA, another asymmetric DMPDA always yielded SAPO-GIS, regardless of the crystallization temperature employed (gel nos. 2 and 10 in Table 1). Here, we considered the strength of intermolecular hydrogen bonding of water to each amine group in the organic compounds with various pK_a values as another crucial factor, in addition to the size and shape (or symmetry) of organic compounds themselves, for the zeotype structure direction.

Indeed, the tertiary amine group of DMEDA, with a pK_a closer to the value of water compared to its primary amine group, should be able to exert stronger hydrogen-bonding interactions with water[29,30], leading to the persistence of this assembly during synthesis of SAPO-PHI, as supported by the AIMD simulations where water molecules were always associated with tertiary aminium group of DMEDAs to form stable 1:1 hydrogen-bonded assemblies at 150 °C (Figure S13). At higher

temperature, a larger decrease in pK_a values is generally observed for tertiary amine groups as compared to the case of primary ones leading to a smaller difference between the values of each amine group[31,32]. Measuring the pK_a values of each amine group *in-situ* is however not straightforward. Nevertheless, the different temperature dependence of the pK_a values can explain the formation of SAPO-CHA using the same DMEDA-mediated synthesis mixture for SAPO-PHI synthesis (i.e. gel no. 2 in Table 1) at the higher crystallization temperature (180 ºC), similar to the case of TMEDA with a pair of tertiary aminium groups possessing the same hydrogen bonding strength toward water. A similar explanation can be given for asymmetric DMPDA and symmetric TMPDA, whose two pK_a values are already more alike than those of the ethylene derivatives[29], so that both direct SAPO-GIS synthesis, regardless of the crystallization temperature (Table 1).

To further confirm the structure-directing role of $[H_2O\text{-}(DMEDA{\cdot}H_2)]^{2+}$ during SAPO-PHI synthesis, we investigated the crystallization kinetics at 150 °C of SAPO-PHI to further confirm the structure-directing role of $[H_2O\text{-}(DMEDA{\cdot}H_2)]^{2+}$ during synthesis (Figure 3). While the powder XRD pattern of the solid isolated after 1 day of heating only displays X-ray reflections from PB, the Al starting material, its ^{1}H MAS NMR spectrum shows a resonance at 4.7 ppm due to water proton even after dehydration under a vacuum (10^{-4} kPa at 200 °C for 6 h). This resonance becomes stronger with crystallization time, while the ^{1}H resonance of unreacted PB at 2.8 ppm disappears. Raman spectroscopy reveals that the two bands at 3040 and 360 cm^{-1} corresponding to the stretching mode of the hydrogen-bonded N-H^+ group in $[H_2O\text{-}(DMEDA{\cdot}H_2)]^{2+}$ and the translational mode of OH groups in PB[33,34], become stronger and weaker with crystallization time, respectively. Therefore, $[H_2O\text{-}(DMEDA{\cdot}H_2)]^{2+}$ is already present at least at the nucleation stage. Moreover, the 2-amino-*N*,*N*,*N*-trimethylethanaminium ion, whose molecular shape and size are essentially identical to those of $[H_2O\text{-}(DMEDA{\cdot}H_2)]^{2+}$, but with the strongly hydrogen-bonded water molecule replaced by a methyl group, was found to hardly direct the synthesis of SAPO-PHI (gel no. 9 in Table 1). This again confirms the role of the hydrogen-bonded water-aminium assembly as an SDA. The same conclusion can be made for MgAPO-PHI, a PHI-type magnesiumaluminophosphate molecular sieve, synthesized using DMEDA. Like Si in as-synthesized SAPO-PHI, Mg in as-synthesized MgAPO-PHI is fully ordered (Figure S19), suggesting that the heteroatom distributions in MeAPO molecular sieves, as well as in SAPO ones, can be optimized by hydrogen-bonded water-organic assemblies.

■ CONCLUSION

In summary, we have rationally designed hydrogen-bonded water-aminium assemblies that play a structure-directing role in the synthesis of phosphate-based molecular sieves, especially of those with perfectly ordered framework heteroatoms. A combination of single-crystal X-ray crystallography, 1D and 2D MAS NMR, and molecular modelling allowed us to demonstrate that a 1:1 supramolecular assembly of water-diprotonated DMEDA ($[H_2O\text{-}(DMEDA{\cdot}H_2)]^{2+}$) leads to the formation of asymmetric *t-phi* and *t-oto* cages in SAPO-PHI, where its framework Si distribution strictly corresponds to the assembly orientation. The concept presented here is applicable to many other organic molecules with fine-tuned combinations of hydrogen-bonding functional groups, and thus offers an opportunity for finding novel zeotypes. It is also possible to extend this water-organic assembly concept towards aluminosilicate zeolites with ordered Al atoms and thus great industrial potential, using concentrated synthesis mixtures with organic compounds containing aminium groups to achieve charged $[N\cdots H\cdots O]^+$ hydrogen bonding with water.

■ ASSOCIATED CONTENT

Supporting Information

The Supporting information is available free of charge at http://pubs.acs.org/doi/xx.xxxx/jacs.xxxxxxx.
Crystallographic, spectroscopic, and molecular modelling data of the zeotype molecular sieves synthesized here, experimental procedures, supporting Figures S1-S19, and supporting Tables S1-S18 (PDF)

Accession Codes

CCDC 1987271-1987276 contain the supplementary crystallographic data for this paper. These data can be obtained free of charge via www.ccdc.cam.ac.uk/data_request/cif, or by emailing data_request@ccdc.cam.ac.uk, or by contacting The Cambridge Crystallographic Data Centre, 12 Union Road, Cambridge CB2 1EZ, UK; fax: +44 1223 336033.

■ AUTHOR INFORMATION

Corresponding Author

Suk Bong Hong - Center for Ordered Nanoporous Materials Synthesis, Division of Environmental Science and Engineering, POSTECH, Pohang 37673, Korea; Email: sbhong@postech.ac.kr

Authors

Sung Hwan Park - Center for Ordered Nanoporous Materials Synthesis, Division of Environmental Science and Engineering, POSTECH, Pohang 37673, Korea
Sambhu Radhakrishnan - Center for Surface Chemistry and Catalysis, Characterization and Application Team (COK-kat), Celestijnenlaan 200 F – box 2461, KU Leuven, 3001 Heverlee, Belgium & NMRCoRe, Celestijnenlaan 200 F – box 2461, KU Leuven, 3001 Heverlee, Belgium
Wanuk Choi - Center for Ordered Nanoporous Materials Synthesis, Division of Environmental Science and Engineering, POSTECH, Pohang 37673, Korea
C. Vinod Chandran - Center for Surface Chemistry and Catalysis, Characterization and Application Team (COK-kat), Celestijnenlaan 200 F – box 2461, KU Leuven, 3001 Heverlee, Belgium & NMRCoRe, Celestijnenlaan 200 F – box 2461, KU Leuven, 3001 Heverlee, Belgium
Kingsley Christian Kemp - Center for Ordered Nanoporous Materials Synthesis, Division of Environmental Science and Engineering, POSTECH, Pohang 37673, Korea
Eric Breynaert - Center for Surface Chemistry and Catalysis, Characterization and Application Team (COK-kat), Celestijnenlaan 200 F – box 2461, KU Leuven, 3001 Heverlee, Belgium & NMRCoRe, Celestijnenlaan 200 F – box 2461, KU Leuven, 3001 Heverlee, Belgium
Robert G. Bell - Department of Chemistry, University College London, 20 Gordon Street, London WC1H 0AJ, UK
Christine E. A. Kirschhock - Center for Surface Chemistry and Catalysis, Characterization and Application Team (COK-kat), Celestijnenlaan 200 F – box 2461, KU Leuven, 3001 Heverlee, Belgium

Complete contact information is available at: https://pubs.acs.org/xx.xxxx/jacs.xxxxxxx

Notes

The authors declare no competing financial interest.

■ ACKNOWLEDGMENT

We acknowledge financial support from the NCRI (2012R1A3A-2048833 and 2021R1A3A-3088711) and FY2019 (2018K2A9A1A-06070020) programmes through the National Research Foundation of Korea and the Flanders Research Foundation (FWO) for supporting Cooperation between Flanders and Korea. EB acknowledges support from the Flemish government, department EWI via the Hermes Fund (AH.2016.134). NMRCoRe acknowledges the Flemish government, department EWI for financial support as International Research Infrastructure (I001321N: Nuclear Magnetic Resonance Spectroscopy Platform for Molecular Water Research). This project has received funding from the European Research Council (ERC) under the European Union's Horizon 2020 research and innovation programme (WATUSO, 834134). We also thank late F. Taulelle (KU Leuven) for helpful discussion and PAL for synchrotron diffraction experiments at beamlines 2D (D. Moon), 5A (H. H. Lee), and 9B (D. Ahn). PAL is supported by MSIP and POSTECH.

■ REFERENCES

(1) Moliner, M.; Rey, F.; Corma, A. Towards the rational design of efficient organic structure-directing agents for zeolite synthesis. *Angew. Chem. Int. Ed*. **2013**, *52*, 13880–13889.

(2) Baerlocher, Ch.; McCusker, L. B. Database of Zeolite Structures. http://www.iza-structure.org/databases/ (accessed July XX, 2022)

(3) Gies, H.; Marler, B. The structure-controlling role of organic templates for the synthesis of porosils in the systems SiO_2/template/H_2O. *Zeolites* **1992**, *12*, 42-49.

(4) Cundy, C. S.; Cox, P. A. The hydrothermal synthesis of zeolites: Precursors, intermediates and reaction mechanism. *Microporous Mesoporous Mater*. **2005**, *82*, 1-78.

(5) Burkett, S. L.; Davis, M. E. Mechanism of structure direction in the synthesis of Si-ZSM-5: an investigation by intermolecular ^{1}H-^{29}Si CP MAS NMR. *J. Phys. Chem.* **1994**, *98*, 4647-4653.

(6) Sheng, Z. *et al*. Observing a zeolite nucleus (subcrystal) with a uniform framework structure and its oriented attachment without single-molecule addition. *Angew. Chem. Int. Ed*. **2021**, *60*, 13444-13451.

(7) Pauling, L. *The Chemical Bond: A Brief Introduction to Modern Structural Chemistry*; Cornell University Press: Ithaca, 1967.

(8) Marcus, Y. Effect of ions on the structure of water: structure making and breaking. *Chem. Rev*. **2009**, *109*, 1346-1370.

(9) Wernet, Ph. *et al*. The structure of the first coordination shell in liquid water. *Science* **2004**, *304*, 995-999.

(10) Breynaert, E. *et al*. Water as a tuneable solvent: a perspective. *Chem. Soc. Rev*. **2020**, *49*, 2557-2569.

(11) Wilson, S. T.; Lok, B. M.; Messina, C. A.; Cannan, T. R.; Flanigen, E. M. Aluminophosphate molecular sieves: a new class of microporous crystalline inorganic solids. *J. Am. Chem. Soc*. **1982**, *104*, 1146-1147.

(12) Lok, B. M.; Messina, C. A.; Patton, R. L.; Gajek, R. J.; Cannan, T. R.; Flanigen, E. M. Silicoaluminophosphate molecular sieves: another new class of microporous crystalline inorganic solids. *J. Am. Chem. Soc*. **1984**, *106*, 6092-6093.

(13) Flanigen, E. M.; Patton, R. L.; Wilson, S. T. Structural, synthetic and physicochemical concepts in aluminophosphate-based molecular sieves. *Stud. Surf. Sci. Catal*. **1988**, *37*, 13-27.

(14) Trotman-Dickenson, A. F. The basic strength of amines. *J. Chem. Soc*.**1968**, 1293-1297.

(15) Hall, Jr. H. K. Correlation of the base strengths of amines. *J. Am. Chem. Soc*. **1957**, *79*, 5441-5444.

(16) Fuller, W. Hydrogen bond lengths and angles observed in crystals. *J. Phys. Chem.* **1959**, *63*, 1705-1717.

(17) Steiner, T. The hydrogen bond in the solid state. *Angew. Chem. Int. Ed*. **2002**, *41*, 48-76.

(18) Shin, J.; Jo, D.; Hong, S. B. Rediscovery of the importance of inorganic synthesis parameters in the search for new zeolites. *Acc. Chem. Res.* **2019**, *52*, 1419-1427.

(19) Yu, J. Synthesis of zeolites. *Stud. Surf. Sci. Catal*. **2007**, *168*, 39-103.

(20) Jeffrey, G. A.; Mitra, J. Three-center (bifurcated) hydrogen bonding in the crystal structures of amino acids. *J. Am. Chem. Soc*. **1984**, *106*, 5546-5553.

(21) Chantrapromma, S.; Usman, A.; Fun, H.-K.; Poh, B.-L.; Karalai, C. The 1:2 adduct *N*,*N*-dimethylethylenediamine-1,4-diium bis(2,4-dinitrophenolate). *Acta Cryst*. **2002**, *E58*, o108-o110.

(22) Bujak, M.; Frank, W. Crystal structure of the inorganic-organic hybrid material bis(*N*,*N*-dimethyl-1,3-diammoniopropane) hexachloridorhodate(III) chloride, $[(CH_3)_2NH(CH_2)_3NH_3]_2[RhCl_6]Cl$, $C_{10}H_{32}Cl_7N_4Rh$. *Z. Kristallogr. NCS* **2014**, *229*, 147-148.

(23) Minor, W.; Cymborowski, M.; Otwinowski, Z.; Chruszcz, M. HKL-3000: the integration of data reduction and structure solution – from diffraction images to an initial model in minutes. *Acta Cryst.* **2006**, *D62*, 859-866.

(24) Sheldrick, G. M. XPREP. Bruker AXS Inc., Madison, Wisconsin, USA, 2003.

(25) Sheldrick, G. M. Phase annealing in SHELX-90: direct methods for larger structures, *Acta Cryst*. **1990**, *A46*, 467-473.

(26) Sheldrick, G. M. A short history of SHELX. *Acta Cryst.* **2008**, *A64*, 112-122.

(27) CP2K version 5.1, the CP2K developers group. https://www.cp2k.org/ (2017).

(28) VandeVondele, J. *et al*. Quickstep: fast and accurate density functional calculations using a mixed Gaussian and plane waves approach. *Comput. Phys. Commun*. **2005**, *167*, 103–128.

(29) Garner, R.; Yperman, J.; Mullens, J.; Poucke, L. Potentiometric determination of the protonation constants of N-methyl substituted ethylene and propylene diamines in 1mol/1KNO_3. *Fresenius' J. Anal. Chem*. **1993**, *374*, 145-146.

(30) Gilli, P.; Pretto, L.; Bertolasi, V.; Gilli, G. Predicting hydrogen-bond strengths from acid-base molecular properties. The pK_a slide rule: toward the solution of a long-lasting problem. *Acc. Chem. Res.* **2009**, *42*, 33-44.

(31) Rayer, A. V.; Sumon, K. Z.; Jaffari, L.; Henni, A. Dissociation constants (pK_a) of tertiary and cyclic amines: structural and temperature dependences. *J. Chem. Eng. Data*. **2014**, *59*, 3805-3813.

(32) Tagiuri, A.; Mohanned M.; Henni, A. Dissociation constants (pK_a) and thermodynamic properties of some tertiary and cyclic amines from (298 to 333) K. *J. Chem. Eng. Data*. **2015**, *61*, 247-254.

(33) Krishnan, R. S.; Krishnan, K. Influence of the hydrogen bond on the N-H stretching frequencies in amino-acids. *Proc. Ind. Acad. Sci*. **1964**, *60*, 11-19.

(34) Assih, T.; Ayral, M.; Abenoza, M.; Phalippou, J. Raman study of alumina gels. *J. Mater. Sci*. **1988**, *23*, 3326-3331.

Table of Contents (TOC)